## Title

ELECTRON ENERGY LOSS AND THERMAL DESORPTION SPECTROSCOPY OF PYRIDINE ADSORBED ON Pt(lll)



## Authors

Grassian, V.H.
Muetterties, E.L.

## Publication Date

1986-02-01

LBL-22042
Preprint

# Lawrence Berkeley Laboratory
UNIVERSITY OF CALIFORNIA

## Materials & Molecular Research Division



To be published in Journal of Physical Chemistry

ELECTRON ENERGY LOSS AND THERMAL DESORPTION SPECTROSCOPY OF PYRIDINE ADSORBED ON Pt(111)

V.H. Grassian and E.L. Muetterties

February 1986



Prepared for the U.S. Department of Energy under Contract DE-AC03-76SF00098

## DISCLAIMER

# Electron Energy Loss and Thermal Desorption Spectroscopy of Pyridine Adsorbed on Pt(111)

V. H. Grassian* and E. L. Muetterties†

Department of Chemistry and
Materials and Molecular Research Division
Lawrence Berkeley Laboratory
University of California
Berkeley, California 94720

* Author to whom correspondence should be addressed
† Deceased, January 12, 1984

Abstract

The chemisorption behavior of pyridine ($NC_5H_5$) on a Pt(111) surface has been examined using thermal desorption and electron energy loss spectroscopy as a function of adsorption temperature. The vibrational spectrum of pyridine adsorbed at room temperature on this surface shows intense loss peaks in the specular direction from vibrational modes which can be characterized as in-plane stretching and bending modes. This vibrational spectrum has been interpreted as the formation of an α-pyridyl species ($NC_5H_4$) on the surface. The pyridyl moeity is bonded to the platinum surface through the nitrogen and one of the α-carbon atoms with the pyridyl plane perpendicular to the metal surface. When pyridine is adsorbed at low temperature (120K), it bonds to the surface through both the nitrogen atom and the $\pi$ and $\pi^*$ orbitals of the pyridine ring. As the crystal is warmed to 260K, at saturation coverage, approximately 50% of the molecules desorb as molecular pyridine. The remaining pyridine molecules partially decompose on the surface to form an α-pyridyl fragment. The electron energy loss spectra of pyridine adsorbed at both low and room temperature is compared to the infrared specta of two osmium cluster compounds $Os_3(CO)_{11}(NC_5H_5)$, a pyridine complex and $HOs_3(CO)_{10}(NC_5H_4)$, a pyridyl complex.

## INTRODUCTION

The bonding of aromatic molecules on many different single crystal metals and different crystallographic planes has been a subject of considerable interest. Benzene has been the most studied aromatic molecule so far and by several different surface science techniques including photoelectron spectroscopy, low energy electron diffraction, thermal desorption spectroscopy (TDS) and electron energy loss spectroscopy (EELS). The adsorption geometry

of benzene on the low Miller index surface planes of many transition metals (Pt, Ni, Pd, Rh, Ir, Ru) has been established fairly conclusively.[1] The ring plane of benzene is oriented parallel to the surface plane. The $\pi$ and $\pi^*$ orbitals of benzene are considered to interact with the metal orbitals in forming the chemisorption bond. In the case of heteroaromatics there is the possibility of a similar interaction between the $\pi$ and $\pi^*$ orbitals of the adsorbate and the metal atoms. However, there is now the possibility of an interaction between the metal and the nonbonding lone pair of electrons localized on the heteroatom which can bond to the surface in a conventional sigma donor type interaction.

The importance of both of these interactions for heteroaromatics adsorbed on metal surfaces has been observed with pyridine on Ag(111) and Ni(100).[2] Both vibrational and electronic electron energy loss spectroscopy of pyridine adsorbed on Ag(111) have shown the conversion of a $\pi$ bonded to nitrogen bonded pyridine as the pyridine coverage is increased. For coverages below 0.50 monolayers, pyridine adsorbs in a flat configuration, i.e. with the ring plane parallel to the surface plane in a geometry similar to that of benzene on the Ag(111) surface. For coverages above 0.5 monolayers there is a "phase transformation" to a nitrogen bonded species. Recently a study by DiNardo *et al.*[2] again using electron energy loss spectroscopy of pyridine adsorbed on Ni(100) showed the existence of two nitrogen bonded species. The surface chemistries of pyridine, deuterium labeled pyridines, and methyl substituted pyridines have been studied on the Ni(100) and Ni(111) surfaces.[3]

The IR and Raman spectra of pyridine and isotopically substituted pyridines have been well studied[4-8] and normal coordinate analysis have been used to assign normal modes to the observed spectral features.[5-7] The infrared spectra of pyridine complexed with a variety of mononuclear

transition metal complexes have been studied as a function of metal and coligands.[9-10] In all of these metal complexes, pyridine is bonded to the metal atom through the nitrogen lone pair. There were only minor shifts, 15-25 $cm^{-1}$, in the vibrational frequencies of pyridine in these complexes relative to that of liquid pyridine. This is in contrast to benzene $\pi$ complexes such as bis benzene chromium, $Cr(C_6H_6)_2$, and benzene chromium tricabonyl, $Cr(C_6H_6)(CO)_3$, where large shifts of 50-150 $cm^{-1}$ from gas phase frequencies are observed for some modes.[11]

We present here a vibrational study using electron energy loss spectroscopy of pyridine adsorbed on Pt(111) as a function of temperature. The complimentary technique of thermal desorption spectroscopy was also employed. The infrared spectrum of two prototype cluster compounds. $OS_3(CO)_{11}(NC_5H_5)$ and $HOs_3(CO)_{10}NC_5H_4$ (and their perdeuterated analogues) were also recorded for comparison. Triosmium and tricobalt cluster compounds have been extremely useful as prototype structural models in identifying adsorbed species on metal surfaces.[12,13,14]

## EXPERIMENTAL

All experiments were performed in a stainless steel ultra-high vacuum (UHV) chamber. The base pressure of the chamber was typically $<2 \times 10^{-10}$ torr. The chamber contained a 200 liter/sec ion pump and an auxillary titanium sublimation pump. The system was equipped with low energy electron diffraction (LEED) optics and Auger electron spectroscopy; the Auger electrons were analyzed with the four grid retarding field analyzer of the LEED optics. A Vaccum Generator quadrupole mass spectrometer was used to monitor individual masses during a thermal desorption spectroscopy experiment as well as background gases in the chamber.

The design of the Electron Energy Loss Spectrometer used in these experiments has been described elsewhere.[15] Briefly the spectrometer consists of two 120° cylindrical sectors, a monochromator and an analyzer. An incident beam energy of 3 eV was used with an energy resolution of 50-80 $cm^{-1}$ ($\Delta E_{FWHM}$). Typically the count rate in the elastic channel was $1 \times 10^5$ counts/sec. For experiments done in the specular direction the angle of the incident and the scattered beam were both 60° with respect to the surface normal. Off-specular measurements were made by rotating the crystal about the vertical axis.

The platinum crystal was spark cut and oriented along the (111) direction using Laue X-ray back diffraction. The crystal, 1 cm in diameter, was then polished according to procedures described by Tsai et al.[16] The crystal was spot-welded to two platinum wires 15 mil in diameter which mounted the crystal to a copper block. The crystal was cooled in a similar manner as described previously with minor modifications.[17] Liquid nitrogen was passed through two copper cold fingers connected by copper braids 5" long and 1/4" in diameter to the copper block on which the sample was mounted. The crystal temperature, as monitored by a chromel-alumel thermocouple spot-welded to the bottom of the crystal, reached a minimum temperature of 120K. The sample was heated resistively through the same copper braids to override the cooling of the crystal. The copper block which mounted the crystal was mechanically attached to a stainless steel manipulator offset 2" from the center of the chamber so the sample could be rotated to any part of the chamber desired. A tilt mechanism permitted the crystal to be rotated on the crystal axis for off-specular electron energy loss measurements.

Pyridine (Mallinckrodt) and pyridine-$d_5$ (99.5% d) (Merck, Sharpe, and Dohme) were used without purification. The isotopically substituted

pyridines, 2,6d$^2$ pyridine and 4d$^1$ pyridine were prepared by the method of Bak et al. and as described elsewhere.[3,18] The pyridine sample was degassed by several freeze-thaw cycles and then introduced into the vacuum chamber. All exposures are uncorrected for ion-gauge sensitivity.

To remove surface carbon, the Pt(111) crystal was heated to 1000K in the presence of oxygen at a pressure of $1 \times 10^{-6}$ torr. After the crystal was free of carbon impurities (as shown by Auger spectra). Sulfur impurities that remained after this treatment can then be removed by heating the crystal to 800K in oxygen again at a pressure of $1 \times 10^{-6}$ torr. Oxygen that remained on the surface after these cleaning treatments was removed by briefly heating the crystal to 1200K. Calcium was removed from the crystal surface by sputtering the surface with argon ions at an Ar pressure of $1 \times 10^{-5}$ and an incident beam energy of 600 eV with the sample temperature at 300K. These procedures were repeated until the surface was determined to be clean by Auger electron spectroscopy. The lattice orientation was determined by low energy electron diffraction.

The tri-osmium cluster compounds were synthesized in a procedure slightly modified from that previously described by Yin et al.[19,20] Standard vacuum and Schlenk line techniques were used in preparation of these compounds: reactions were carried out under an atmosphere of nitrogen. Using 300 mg of $Os_3(CO)_{12}$ (Strem Chemicals) dissolved in 100 mls of methylene chloride, excess of reagent grade pyridine (or perdeuterated pyridine), 1 ml, was transferred into the reaction flask. A solution of trimethylamine oxide $(CH_3)_3NO$ (35 mg $(CH_3)_3NO$ dissolved in 35 mls of $CH_2Cl_2$) was added dropwise to the osmium reaction mixture. The progress of the reaction was monitored by infrared spectroscopy in the 2100-1700 $cm^{-1}$ region where carbonyl absorption occurs. Trimethylamine oxide was added until the 2070 $cm^{-1}$ band corresponding to the

reactant, $Os_3(CO)_{12}$ disappeared. The solvent was pumped off, the product $Os_3(CO)_{11}(NC_5H_5)$ was redissolved in methylene chloride and pentane and then recrystallized. The solvent was decanted and evaporated off under vacuum.

The product $Os_3(CO)_{11}(NC_5H_5)$ (100 mg) was used in the preparation of the pyridyl complex, $HOs_3(CO)_{10}(NC_5H_4)$. $Os_3(CO)_{11}(NC_5H_5)$ was dissolved in 50 mls of n-octane containing a few drops of pyridine, and the mixture was refluxed for one hour. The pyridyl complex was isolated by chromatography using a silica column and pentane elutant. After the compound was collected, the solvent was evaporated.

The infrared spectra of both these compounds were recorded over the spectral range 400-3200 $cm^{-1}$ using a Perkin Elmer 283 infrared spectrometer with a spectral resolution of 2-3 $cm^{-1}$ and a frequency accuracy of 1-2 $cm^{-1}$. Anhydrous KBr was used in the preparation of the KBr discs.

## RESULTS

### Infrared Spectra of $Os_3(CO)_{11}(NC_5H_5)$ and $HOs_3(CO)_{10}NC_5H_4$

We present the infrared spectra recorded for $Os_3(CO)_{11}(NC_5H_5)$ (**1a**) and $HOs_3(CO)_{10}(NC_5H_4)$ (**1b**) first so we may use these results when discussing the electron energy loss spectrum recorded for pyridine adsorbed on Pt(111).

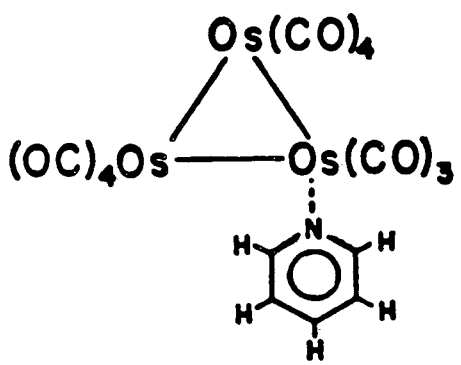


**1a**

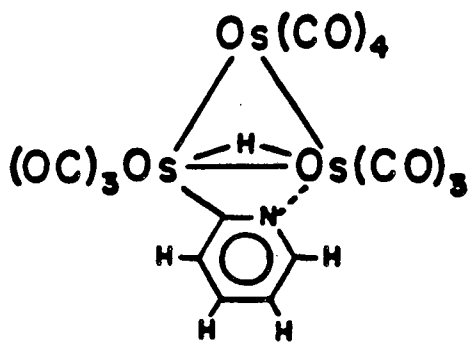


**1b**

Figure **1a** shows the infrared spectra in the spectral range from 400 to 1650 $cm^{-1}$ for the two osmium cluster compounds. The infrared spectra for the perdeuterated analogues are shown in Figure **1b**. In both the pyridine and the pyridyl triosmium complexes the pyridine moiety is bonded to one of the metal atoms in the cluster through the nitrogen. In the pyridyl complex the pyridine moiety is additionally bonded to the metal cluster through the α carbon.

In Table I we list the low frequency absorption bands (400-610 $cm^{-1}$) for the pyridine and pyridyl cluster compounds along with the corresponding frequencies for $Os_3(CO)_{12}$.[21] The comparison of the low frequency bands observed in the IR spectra (Fig. 1) of the two prototype model compounds (**1a** and **1b**), match reasonably well to the observed absorption bands in the IR spectra of $Os_3(CO)_{12}$. Thus verifying that these absorptions are associated with the bending and stretching modes of the metal framework, the metal carbon stretching motion and the metal carbonyl bending motions. The spectral region from 600-1650 $cm^{-1}$ is of more interest in this study, the absorption bands which occur at these frequencies are due to the vibrations of the pyridine and pyridyl fragments of the cluster. The assignment for the bands in this region are made by comparison to the vibrational spectrum and the assignment made for liquid pyridine (Table II). The frequencies of the absorption bands for these cluster compounds compare well with the vibrational frequencies for uncomplexed pyridine. The correspondence of the spectral features between pyridine and complexed pyridine (or pyridyl) permits the use of liquid phase vibrational assignments for guidance as we interpret the spectral observations. The average frequency shift from liquid pyridine frequencies is calculated to be 13 $cm^{-1}$ for the pyridine complex (**1a**). As would be expected the frequencies of the vibrations of the pyridyl fragment do not correlate as well

to liquid pyridine frequencies with an average frequency shift of 27 $cm^{-1}$. However, qualitatively these infrared spectra confirm that the fingerprint regions for pyridine and pyridyl are reasonably similar if looked at with sufficiently low resolution, as is the case of a vibrational spectrum recorded using the technique of electron energy loss spectroscopy.

ROOM TEMPERATURE ADSORPTION OF PYRIDINE ON Pt(111)

I. Electron Energy Loss Spectroscopy

The electron energy loss spectrum recorded in the specular direction of pyridine adsorbed at room temperature onto platinum (the 111 surface) is shown in Figure **2a**. Loss peaks listed in order of decreasing frequency are observed at 3080, 1570, 1450, 1230, 1150, 1010, and 740 $cm^{-1}$. Perdeuteropyridine, similarly studied (Fig. **2b**), displays loss peaks in the specular direction, in order of decreasing frequency, at 2275, 1540, 1330, 1230, 1010, 860, and 680 $cm^{-1}$. Table III lists these frequencies with their liquid phase counterparts, again we feel that their correspondence to liquid phase pyridine permit the use of liquid phase vibrational assignments as a guide.

One of the most significant aspects to the spectrum in Figure 2 is the prominence of the loss at 3080 $cm^{-1}$. The frequency and the deuterium shift to 2275 $cm^{-1}$ definitively identify the characteristic aromatic C-H stretching motion. Since C-H stretching modes are intrinsically in-plane vibrations, their intensity in the specular direction indicates that pyridine is not adsorbed with its skeletal plane parallel to the metal surface. This conclusion is strengthened by the high intensities observed in the spectral region 1000-1600 $cm^{-1}$ where C-C stretching and C-H in plane bending modes occur. It is also consistent with the striking difference from the corresponding spectra of benzene[22] and toluene[23] on platinum (111) surfaces.

These substances, when adsorbed, have EELS spectra with extremely weak loss features both in the C-H aromatic stretching region and in the 1000-1600 $cm^{-1}$ range.

The electron energy loss spectrum of two specifically labeled pyridines. $4d^1$ pyridine and $2,6d^2$ pyridine adsorbed on Pt(111) at 300K have also been measured. In Figure 3 we show the EELS spectrum in the spectral region from 2000 to 3200 $cm^{-1}$ for these two specifically labeled compounds along with the EELS spectrum for normal and perdeuterated pyridine in the same region for reference. There is a large difference in the intensities of the loss peaks associated with the C-D and C-H stretching motion between the two compounds $4d^1$ pyridine and $2,6d^2$ pyridine. The intensity of the loss peak at 2275 $cm^{-1}$ (the C-D stretching mode) is very weak in the specular direction for $2,6d^2$ pyridine. The intensity of this loss peak increases when the sample is tilted 10° off the specular angle. Clearly this loss peak is non-dipolar in nature. This is in contrast to $4d^1$ pyridine where there is a significant dipole contribution to the intensity of the loss peak. The results from these specifically labeled compounds will be useful in determining the orientation and adsorption geometry of the pyridine ring.

## II. Thermal Desorption Spectroscopy

The thermal desorption spectrum of pyridine adsorbed on Pt(111) at room temperature is shown in Figure 4. This figure shows the trace of the parent ion which corresponds to an AMU of 79. There is one molecular desorption peak in the thermal desorption curve, this peak has a temperature desorption rate maximum at approximately 473K. As the coverage is increased the intensity of the peak also increases until saturation coverage is reached.

The decomposition of pyridine as monitored by the thermal desorption

hydrogen curves for pyridine, $d^5$ pyridine, $4d^1$ pyridine, $2,6d^2$ pyridine, and $3,5d^2$ pyridine has been discussed previously.[3] For normal pyridine ($NC_5H_5$) there are three hydrogen peaks in the thermal desorption spectrum. The desorption rate temperature maxima for these peaks occur at approximately 335K, 515K, and 620K. Through the use of the specifically labeled pyridines it was determined that the low temperature hydrogen (deuterium) peak was due to carbon-hydrogen bond cleavage at the α-carbon only. The regiospecific bond breaking of the α carbon-hydrogen bond led the authors to suggest the formation of an α-pyridyl intermediate, although no spectroscopic evidence was available at that time. The intensity ratio of the hydrogen desorption peaks was 0.5:2:2 for the 335K, 515K, and 620K peaks, respectively. The deviation from one of the low temperature peak was attributed to the observation of immediate hydrogen desorption upon pyridine adsorption. Our results on the decomposition of pyridine on Pt(111) is in qualitative agreement with these earlier results. Figure 7 shows $H_2$ desorption from low temperature pyridine adsorption, which will be discussed further in the next section. $H_2$ evolution for room temperature pyridine adsorption is similar except for the intensity of the first desorption maxima which is approximately one-half in the room temperature spectrum.

The amount of irreversibly bound pyridine can be calculated using the peak-to-peak height ratios of the carbon 272 eV Auger electron peak relative to the platinum 237 eV Auger electron peak. An Auger spectrum was taken after the crystal first was exposed to pyridine to reach saturation coverage which was then compared to the Auger spectrum taken after the thermal desorption experiment. The amount of carbon on the surface was calculated using equation (1).[24]

$$\frac{I(272)}{I(237)} \times 0.64 = \Theta_{carbon} \qquad (1)$$

The amount of pyridine which irreversibly adsorbs was calculated to be approximately 60% ± 5% for pyridine adsorbed at room temperature.

LOW TEMPERATURE ADSORPTION OF PYRIDINE ON Pt(111)

I. Electron Energy Loss Spectroscopy

The electron energy loss spectrum recorded for pyridine adsorbed on Pt(111) at 120K and saturation coverage is shown in Figure 5. This spectrum is substantially different than the spectrum for pyridine adsorbed at room temperature. Loss peaks are observed in order of decreasing frequency at: 3070, 1610, 1470, 1230, 1050, 840, and 660 $cm^{-1}$. And for perdeuteropyrdine adsorbed on this platinum surface at 120K loss peaks are observed at 2270, 1570, 1330, 1250, 1010, 830, 580, and 290 $cm^{-1}$. For monolayer or submonolayer quantities of pyridine adsorbed on the Pt(111) surface at 120K we again find most of the modes observed in the specular direction can be characterized as primarily in-plane modes, as was seen in the room temperature spectrum. The relative intensities of the loss peaks differ greatly between spectra for room temperature and low temperature adsorption of pyridine. In addition to intensity differences between the EELS spectrum for pyridine adsorption at 120K and 300K we find no loss peak at 740 $cm^{-1}$ in the low temperature EELS spectrum of normal pyridine. There are two new loss peaks observed in the low temperature spectrum at 660 $cm^{-1}$ and 840 $cm^{-1}$. In Table III the vibrational frequencies for pyridine adsorbed on Pt(111) at 120K are compared to the vibrational frequencies for uncomplexed liquid or gas phase values of pyridine.

II. Thermal Desorption Spectroscopy

Figure 6 shows the thermal desorption spectrum of pyridine adsorbed at 120K, again monitoring the parent ion (AMU=79) as a function of coverage. At low coverages there are two molecular desorption peaks. As the coverage increases the intensity of the low temperature peak increases with coverage and the temperature of the rate maxima shifts to lower temperature. At low coverages (0.1 monolayers) $T_{max}$ = 347K, the maxima shift to a $T_{max}$ of 260K at saturation coverage. The high temperature peak with a $T_{max}$ = 483K at $\theta$=0.11 shifts down to $T_{max}$ = 450K at $\theta$=4.0. As the coverage increases a third desorption peak develops with a temperature desorption rate maximum at 190K. As the coverage is increased further, this is the only peak which increases in intensity.

The amount of pyridine which irreversibly adsorbs decreases when pyridine is adsorbed at low temperatures. The amount of decomposition is calculated using equation 1 to be 25%. This is approximately more than two-fold less than the amount of irreversible desorption when pyridine is adsorbed at room temperature. The thermal desorption hydrogen curve, for saturation coverage, is shown in Figure 7. Three peaks are observed in the spectrum with temperature maxima of 335K, 515K, and 620K.

## DISCUSSION

### Room Temperature Adsorption

The $C_{2V}$ molecular symmetry of normal pyridine and $d^5$ pyridine breaks up the 27 fundamental modes of vibration into the irreducible representation as follows: $10a_1$, $3a_2$, $9b_1$, and $5b_2$ modes. The $A_2$ modes are Raman active only and the $A_1$, $B_1$, and $B_2$ modes are both infrared and Raman active. The $A_2$ and $B_2$ modes are out-of-plane modes and the 19 $A_1$ and $B_1$ modes are in-plane

modes. The key question in this study is which modes will be active for pyridine adsorbed on the Pt(111) surface. To answer it, we take advantage of the fact that the infrared spectra recorded for the two cluster compounds $Os_3(CO)_{11}(NC_5H_5)$ and $HOs_3(CO)_{10}(NC_5H_4)$ were similar enough in the 600-1650 $cm^{-1}$ region for the use of liquid pyridine absorption frequencies in the interpretation of orientation of the molecule on the surface regardless of whether it is pyridine or pyridyl on the surface. The EELS active modes will be dependent on the adsorption site and the orientation of the molecule on the surface. The surface normal dipole selection rule states that only modes which are totally symmetric with respect to all symmetry elements ($A_1$ modes) will be dipole active and therefore be strongly dependent on scattering angle. The intensity of those loss peaks will be at a maximum in the specular direction in the EELS spectrum if there is a significant dipole scattering contribution to the cross section of the loss peak. The symmetry of the pyridine-platinum complex can retain the $C_{2V}$ symmetry of molecular pyridine or it can be reduced to $C_S$ symmetry. If the pyridine molecule was nitrogen bonded to the surface and tilted at some angle away from the surface or lying in a flat configuration $\pi$-bonded parallel to the surface the only symmetry element would be the mirror plane perpendicular to the molecular plane that bisects the nitrogen atom and the C-H unit in the 4 position. If there was partial decomposition of the pyridine molecule to form a pyridyl fragment, $(NC_5H_4)$, the point group symmetry of the pyridyl fragment would again be $C_S$ but now the molecular plane would be the mirror plane. In this case both the $A_1$ and $B_1$ irreducible representations of the $C_{2V}$ point group would be lowered to the A' irreducible representation of the point group $C_S$ and the vibrations of this representation would be "EELS allowed".

In Table III we show the frequencies for the normal modes of vibration of uncomplexed pyridine and compare these frequencies to the frequencies observed in the electron energy loss spectrum for pyridine adsorbed at 300K on the Pt(111) surface. Due to the poor resolution of EELS the frequencies of some of the modes have been used more than once in assigning the spectrum of adsorbed pyridine. Also some of the vibrations which are inherently weak transitions (i.e. weak absorption bands in the infrared spectrum of liquid phase pyridine) are not observed. There is some uncertainty in the assignment of the loss peak at 740 $cm^{-1}$ in the pyridine EELS spectrum. This loss peak might be assigned to either of the strong absorptions at 700 $cm^{-1}$ ($\nu_{26}$) or 744 $cm^{-1}$ ($\nu_{25}$) for pyridine in the liquid phase which are assigned to out-of-plane motions of a pyridine. However, the corresponding loss peak in the $NC_5D_5$ spectrum (Fig. 2b) at 685 $cm^{-1}$ displays a deuterium shift by a factor of only 1.08, much smaller than those displayed for liquid pyridine, 1.18 for $\nu_{25}$ amd 1.33 for $\nu_{26}$. Hence, the 740 $cm^{-1}$ loss peak is assigned to the $B_1$ $\nu_{19}$ mode which implies that this mode shifts up in frequency by 13%. In the pyridyl molecular complex the $\nu_{19}$ mode is assigned to the band at 708 $cm^{-1}$ and is therefore also shifted to higher frequency, here by 9%. It is unclear why this low frequency in-plane ring deformation would be more perturbed than other in-plane ring modes in the pyridyl structure. A detailed force-field coordinate analysis would perhaps answer this question.

As noted previously there are intense in-plane modes in the electron energy loss spectrum for pyridine adsorbed at 300K on the Pt(111) surface. As shown in Table III the modes observed in this spectrum are modes of $A_1$ and $B_1$ type symmetry, i.e. in-plane modes. These in-plane modes have high intensity at the specular angle, so they are the one with significant dipole derivatives perpendicular to the platinum surface.

The results for the specifically labeled pyridines support the proposal of the presence of a pyridyl fragment on the surface at room temperature. If only a dipolar contribution to the intensities of the loss peaks for the C-D stretching modes and the C-H stretching modes is considered in the specular direction, the expected intensity ratio for the C-H stretching mode relative to the C-D stretching mode depends upon the component of $\frac{d\mu}{dr}$ perpendicular to the metallic surface and the fact that $(\frac{d\mu}{dr})_{C-H} = 2(\frac{d\mu}{dr})_{C-D}$. For a "stand up" geometry with the N-Pt bond perpendicular to the metallic surface, this ratio $\frac{I_{C-H}}{I_{C-D}}$ is predicted to be 4 for both the 2,6-dideutero and 4-monodeutero pyridines. For a geometry with one of the N-C bonds parallel to the metallic surface, the ratio $\frac{I_{C-H}}{I_{C-D}}$ is predicted to be infinity for the 2,6-dideuteropyridine (one of the deuterium atoms being lost to form an α C-Pt bond) and it would be 2 for the 4-monodeutero pyridine. The spectra in Figure 2 show for the 2,6-dideutero pyridine a very small C-D feature (at specular reflection) with a ratio $\frac{I_{C-H}}{I_{C-D}} = 10$. For the 4-monodeutero pyridine the experimental ratio is about 1.5. Thus the spectra distinctly favor the parallel N-C bond geometry with the loss of an α hydrogen to permit platinum bonding to both the nitrogen and one of the α carbon atoms.

In the case of room temperature adsorption of pyridine on Pt(111) the predominant reaction scheme proposed based on the evidence presented is:

$$NC_5H_5(g) + Pt(111) \xrightarrow{T = 300K} NC_5H_4 - Pt(111) + H-Pt(111)$$

$$2H - Pt(111) \xrightarrow[(T > 300K)]{\Delta} H_2(g)$$

$$2NC_5H_4 - Pt(111) \xrightarrow[(T > 425K)]{\Delta} NC_5H_5(g) + 3/2\ H_2(g) + Pt(111) - N,5C$$

An α-pyridyl species is formed upon pyridine adsorption on the Pt(111) surface. Atomic hydrogen on the surface desorbs as $H_2$ with a $T_{max} = 335K$.

The pyridyl structure was determined by electron energy loss spectroscopy to be stable up to a temperature of 425K. When the temperature is increased above 425K, disproportionation must occur, as revealed by the desorption of molecular pyridine (see Figure 4). Some pyridyl fragments undergo further decomposition. The available hydrogen from this process can then recombine with a remaining pyridyl fragment which then desorbs as molecular pyridine (AMU = 79). Although hydrogen evolution peaks at a somewhat higher temperature ($T_{max}$ = 515K (see Figure 7)) then the pyridine desorption peak (T = 473K), the two processes, decomposition and desorption, begin at about the same temperature, near 425K.

Low Temperature Adsorption

The assignment for low temperature monolayer or submonolayer pyridine covered surface is also given in Table III. The loss peak observed at 660 $cm^{-1}$ is assigned to the $\nu_{19}$ ring deformation mode, close to the liquid phase value, 652 $cm^{-1}$, but distinctly different from 740 $cm^{-1}$ in the room temperature spectrum. The loss peak at 840 $cm^{-1}$ (which shifts to 580 $cm^{-1}$ for $d^5$ pyridine) is assigned to the $\nu_{26}$ mode which corresponds to an in-phase out-of-plane bending motion. The increase of the C-H out-of-plane bending mode relative to the frequency of the free molecule is also observed for benzene adsorbed on Pt(111).[22] The plane of the pyridine molecules is tilted from the surface plane as is suggested by the relative intensities of the in-plane modes. Although the pyridine ring is tilted away from the surface plane there is still an appreciable interaction with the surface metal d orbitals and the $\pi$ and $\pi^*$ orbitals of pyridine. This can be seen by the increase in frequency of the C-H out-of-plane bend from 700 $cm^{-1}$ for liquid pyridine to 840 $cm^{-1}$ for pyridine adsorbed on Pt(111) at 120K. At saturation coverage, a value of 52°

has been calculated for the angle between the pyridine ring and the Pt surface plane from Near Edge X-Ray Absorption Fine Structure data.[25] This is consistent with the electron energy loss spectroscopy results presented here. The bonding of pyridine to the surface at low temperatures appears to be through both the lone pair of electrons which are localized on the nitrogen atom and the delocalized molecular $\pi$ orbitals on the ring. The lowest energy configuration is then a combination of these two different modes of bonding.

The thermal desorption spectrum for pyridine adsorbed on Pt(111) at a temperature of 120K shows three molecular desorption peaks. The low temperature (190K) peak which begins to appear only at coverages greater than a monolayer is attributed to the desorption of multilayer pyridine. Using Redheads equation for first-order reaction kinetics,[26] and assuming a pre-expotential factor of $10^{13}$ $sec^{-1}$, for a temperature maximum of 190K the desorption energy was calculated to be 10.8 kcal/mole. The second molecular pyridine desorption peak has a temperature maximum which is coverage dependent (low coverages $T_{max}$ = 347K; saturation coverage $T_{max}$ = 260K), such behavior could be caused by a second order desorption process which follows second order reaction kinetics or a first order desorption process with an energy of activation that is coverage dependent. A first-order process with a coverage dependent energy of activation is the more probable cause of the variaton of the temperature maximum as a function of coverage, due to the low mobility of the pyridine molecule at these temperatures. Again using a pre-expotential factor of $10^{13}$ $sec^{-1}$ the energy of activation at low coverages is calculated to be 21.8 kcal/mole while at saturation coverage the energy of activation drops to 15.0 kcal/mole. The high temperature molecular desorption peak with a desorption rate maximum centered at T=483K at $\Theta$=0.11L which shifts to T=450K at $\Theta$=4.0L is the only molecular desorption peak for pyridine adsorbed at room

temperature. This peak discussed previously for room temperature results corresponds to the disproportionation of a $NC_5H_4$ fragment with a hydrogen atom which then desorbs as molecular pyridine.

For low temperature adsorption when the substrate is warmed the following reaction scheme is observed:

$$NC_5H_5(g) + Pt(111) \xrightarrow{T = 120K} NC_5H_5 - Pt(111)$$

$$2NC_5H_5 - Pt(111) \xrightarrow{\Delta} NC_5H_5(g) + H\text{-}Pt(111) + NC_5H_4 - Pt(111)$$

$$2H - Pt(111) \xrightarrow{\Delta} H_2(g)$$

$$2NC_5H_4 - Pt(111) \xrightarrow{\Delta} NC_5H_5(g) + 3/2\ H_2(g) + Pt(111) - N,5C$$

Initally the pyridine adsorbs on the surface through the nitrogen atom, which presumably acts as a convential electron donor. Then as the sample is warmed some pyridine desorbs molecularly, with the temperature maximum of the desorption rate depending on the initial coverage. At saturation coverage approximately 50% of the pyridine desorbs from the surface at 260K. The remaining adsorbed pyridine molecules fragment to form the pyridyl-surface complex at ~T=300K. On further heating the behavior is identical to that observed for pyridine adsorbed at room temperature. The recombination of a hydrogen atom and a $NC_5H_4$ fragment to desorb as molecular pyridine at temperatures greater than 400K. The amount of pyridine desorbing in this high temperature peak and the amount of decomposition is less when pyridine is adsorbed at low temperature. This supports the earlier conclusion that disproportionation of the pyridyl complex occurs when the temperature is raised above 400K.

The infrared spectra for the two cluster compounds provide additional supportive evidence for the proposed structure of pyridine adsorbed on Pt(111) at 120K and 300K. The absorption bands of the pyridine and pyridyl complexes

which shift the most in frequency are the ones that offer the best differentiation, but superimposed on that must be the certainty with which the assignment can be made. The second factor causes the bands at 1483 $cm^{-1}$, $\nu_5$, and 1474 $cm^{-1}$, $\nu_{14}$, (frequencies for liquid pyridine) to be the first choice. For the pyridine complex (**1a**) $\Delta\nu$ ($\nu_{complex} - \nu_{pyridine\ liquid}$) is 7 $cm^{-1}$ and 10 $cm^{-1}$ for $\nu_5$ and $\nu_{14}$ respectively, and for the pyridyl complex (**1b**) $\Delta\nu$ is -24 $cm^{-1}$ and -21 $cm^{-1}$ again for $\nu_5$ and $\nu_{14}$ respectively. Now looking at the frequencies of the loss peaks in the EELS spectra we observe $\nu_5$ and $\nu_{15}$ (unresolved in EELS spectrum), for pyridine adsorbed at 120K, to be at 1470 $cm^{-1}$ for pyridine adsorbed at 300K these modes are observed at 1450 $cm^{-1}$. This loss peak is then 20 $cm^{-1}$ higher in frequency for pyridine adsorbed at 120K relative to pyridine adsorbed at 300K. Following this comparison, with modes $\nu_4$ (1583 $cm^{-1}$) and $\nu_{13}$ (1581 $cm^{-1}$), for the pyridine complex (**1a**) $\nu_4$ increases by 30 $cm^{-1}$ and $\nu_{13}$ decreases by 3 $cm^{-1}$ relative to liquid pyridine, for the pyridyl complex $\nu_4$ increases by 9 $cm^{-1}$ and $\nu_{13}$ decreases by 32 $cm^{-1}$, again relative liquid pyridine frequencies. A net effect of an increase in frequency in this region for pyridine and a decrease in this region for pyridyl. The loss peak in the EELS spectrum at 1610 $cm^{-1}$ for pyridine absorbed at 120K has increased in frequency by ~30 $cm^{-1}$, and the loss peak for pyrdine adsorbed at 300K has decreased in frequency, relative to liquid pyridine by 12 $cm^{-1}$.

The in-plane ring distortion mode $\nu_{19}$ at 652 $cm^{-1}$ in pyridine shifts very little in the pyridine complex at 650 $cm^{-1}$. In the EELS spectrum for pyridine adsorbed at 120K this mode is assigned to the loss peak at 660 $cm^{-1}$ which is similary unperturbed relative to liquid pyridine. In the pyridyl complex this mode shifts dramatically to 708 $cm^{-1}$, an increase of 56 $cm^{-1}$ relative to the liquid pyridine value. As noted previously a similar behavior is observed for

pyridine adsorbed at room temperature, the $\nu_{19}$ mode has been assigned to the loss peak at 740 $cm^{-1}$. Lastly there is a large increase in the intensity of the adsorption in the perdeutero pyridine complex in the 800 $cm^{-1}$ region shifted from the 1100 to 1200 $cm^{-1}$ region in the perhydro pyridine cluster compound. A similar increase is observed in the 800 $cm^{-1}$ region for low temperature perdeutero pyridine EELS spectrum.

## CONCLUSIONS

The surface chemistry of pyridine on Pt(111) has been studied as a function of temperature. We have shown in the case of room temperature adsorption that there is partial decomposition of the pyridine molecule with an α-hydrogen abstracted, thereby forming a pyridyl surface species. For low temperature adsorption, pyridine adsorbs molecularly with the ring plane tilted toward but not parallel to the surface plane. A new reaction channel is seen for low temperature adsorption from the thermal desorption data. As the temperature is increased from 120K to approximately 260K (this temperature is dependent on the initial pyridine coverage) 50% of the pyridine desorbs as molecular pyridine. The remaining pyridine molecules form a pyridyl surface complex at about room temperature. The infrared spectra recorded for $Os_3(CO)_{11}(NC_5H_5)$ and $HOs_3(CO)_{10}(NC_5N_4)$ aided in the interpretation of the EELS data for the pyridine-platinum system.

Acknowledgement

This work was supported by the National Science Foundation Grant #CHE-83-07159 and by the Director, Office of Energy Research, Office of Basic Energy Sciences, Chemical Sciences Division of the U.S. Department of Energy under Contract No. DE-AC0376SF00098. We would like to thank Deiter Himmelreich for the guidance in preparing the Osmium cluster compounds. We would also like to thank G.C. Pimentel for his guidance in preparing this manuscript. Registry No. Pyridine 110-86-1: Pt. 7440-06-4

Table I

Corresponding Frequencies of the Low Frequency Modes (400-610 $cm^{-1}$) for Tri-Osmium Complexes

| $Os_3(CO)_{12}$[a] | $Os_3(CO)_{11}(NC_5H_5)$ | $HOs_3(CO)_{10}(NC_5H_4)$ |
|---|---|---|
| 400 W[b] | 405 | 403 |
| 410 S | 417 | 412 |
| 429 M | 435 | 439 |
| 448 W | | 451 |
| 462 S | 460 | |
| 474 W | 474 | 483 |
| 496 S | 493 | 498 |
| 516 W | 502 | |
| 534 W | 528,529 | 540 |
| 562 M | 564 | 574 |
| 583 S | 591 | 588 |
| 606 S | 605 | 605 |

[a] Reference: S.F.A. Kettle and P.L. Strangelin, Inorganic Chemistry, Vol. 18, 2749 (1979)

[b] W=weak, M=medium, S=strong

Table II

Vibrational Assignment of $Os_3(CO)_{11}(NC_5H_5)$ and $HOs_3(CO)_{10}(NC_5H_4)$

(600 - 1650 $cm^{-1}$)

| Symmetry | Mode No. | | Description | $NC_5H_5(NC_5D_5)$[C] | | $Os_3(CO)_{11}(NC_5H_5)$ $h^5$ | $(d^5)$ | $HOs_3(CO)_{10}(NC_5H_4)$ $h^4$ | $(d^4)$ |
|---|---|---|---|---|---|---|---|---|---|
| $A_1$ | 4 | (8a)[B] | C-C, C-N Stretch | 1583 | (1554) | 1613 | (1571) | 1592 | (1554) |
| | 5 | (19a) | C-C, C-N Stretch | 1483 | (1340) | 1490 | (1346) | 1459 | (1339) |
| | 6 | (9a) | C-H in-plane bend | 1218 | (882) | 1223 | (896) | 1222 | (869) |
| | 7 | (18a) | C-H in-plane bend | 1072 | (823) | 1075 | (838) | 1082 | (869) |
| | 8 | (12) | asymmetric ring breathing | 1032 | (1014) | 1050 | (1042) | 1057 | (1055) |
| | 9 | (1) | ring breathing | 991 | (963) | 1019 | (979) | 1029 | (1000) |
| | 10 | (6a) | in-plane ring distortion | 601 | (579) | 639 | A | 680 | A |
| $B_2$ | 23 | (5) | o.o.p. ring distortion | 1007 | (828) | 1019 | (838) | 1029 | (869) |
| | 24 | (10b) | o.o.p. ring distortion | 936 | (765) | | (783) | | (738) |
| | 25 | (4) | C-H o.o.p. bend | 744 | (631) | 762 | (650) | 758 | (680) |
| | 26 | (11) | C-H in-phase o.o.p. bend | 700 | (526) | 710 | (540) | 745,740 | (549) |
| | 27 | (16b) | ring o.o.p. distortion | 403 | (367) | | A | | A |
| $B_1$ | 13 | (8b) | C-C, C-N stretch | 1581 | (1546) | 1578 | (1564) | 1549 | (1519) |
| | 14 | (19b) | C-C, C-N stretch | 1442 | (1303) | 1452 | (1328) | 1421 | (1298) |
| | 15 | (14) | C-C ring stretch | 1362 | (1046) | | | | |
| | 16 | (3) | C-C in-plane bend | 1227 | (1226) | | | 1269 | (1216) |
| | 17 | (15) | C-H in-plane bend | 1143 | (856) | 1161 | (843) | 1162,1117 | (825) |
| | 18 | (18b) | C-H in-plane bend | 1079 | (835) | 1075 | (838) | 1082 | (869) |
| | 19 | (6b) | in-plane ring distortion | 652 | (625) | 650 | A | 708 | 632 |

A. Hidden under more intense absorption bands from low frequency vibrations not due to the pyridine moiety.
B. Wilson Mode Numbers for Benzene
C. Colson, S.D., J. Phys. Chem. 88, 6067 (1984).

Table III

Vibrational Frequencies and Assignment for the Electron Energy Loss Spectra of Pyridine and $d^5$ Pyridine Adsorbed on on Pt(111)

| Symmetry | Mode No. | Description | $NC_5H_5(NC_5D_5)$[A] | | Pyridine-Pt(111) T=300K | | Pyridine-Pt(111) T=120K | |
|---|---|---|---|---|---|---|---|---|
| | | | | | $h^5$ | $(d^5)$ | $h^5$ | $(d^5)$ |
| $A_1$ | 1 (2)[B] | C-H stretch | 3094 | (2302) | 3080 | (2275) | 3070 | (2270) |
| | 2 (13) | C-H stretch | 3072 | (2276) | 3080 | (2275) | 3070 | (2270) |
| | 3 (20A) | C-H stretch | 3030 | (2268) | 3080 | (2275) | 3070 | (2270) |
| | 4 (8a) | C-C, C-N stretch | 1583 | (1554) | 1570 | (1540) | 1610 | (1570) |
| | 5 (19a) | C-C, C-N stretch | 1483 | (1340) | 1450 | (1330) | 1470 | (1330) |
| | 6 (9a) | C-H in-plane bend | 1218 | (882) | 1150 | (860) | 1230 | (830) |
| | 7 (18a) | C-H in-plane bend | 1072 | (823) | | | | |
| | 8 (12) | asymmetric ring breathing | 1032 | (1014) | 1010 | (1010) | 1050 | (1010) |
| | 9 (1) | ring breathing | 991 | (963) | 1010 | (1010) | 1050 | (1010) |
| | 10 (6a) | in-plane ring distortion | 601 | (579) | | | | |
| $B_2$ | 23 (5) | o.o.p. ring distortion | 1007 | (828) | | | | |
| | 24 (10b) | o.o.p. ring distortion | 936 | (765) | | | | |
| | 25 (4) | C-H o.o.p. bend | 744 | (631) | | | | |
| | 26 (11) | C-H in-phase o.o.p. bend | 700 | (526) | | | 840 | (580) |
| | 27 (16b) | ring o.o.p. distortion | 403 | (367) | | | | |
| $B_1$ | 11 (20b) | C-H stretch | 3087 | (2289) | 3080 | (2275) | 3070 | (2270) |
| | 12 ( 7b) | C-H stretch | 3042 | (2256) | 3080 | (2275) | 3070 | (2270) |
| | 13 ( 8b) | C-C, C-N stretch | 1581 | (1546) | 1570 | (1540) | 1610 | (1570) |
| | 14 (19b) | C-C, C-N stretch | 1442 | (1303) | 1450 | (1330) | 1470 | (1330) |
| | 15 (14) | C-C ring stretch | 1362 | (1046) | | | | |
| | 16 ( 3) | C-C in-plane bend | 1227 | (1226) | 1230 | (1230) | 1230 | (1250) |
| | 17 (15) | C-H in-plane bend | 1143 | (856) | 1150 | (860) | | |
| | 18 (18b) | C-H in-plane bend | 1079 | (835) | | | 1050 | (830) |
| | 19 ( 6b) | in-plane ring distortion | 652 | (625) | 740 | (685) | 660 | c |
| | | | | | | | νPT-N | (290) |

A. Pyridine Frequencies and Assignments Taken From: Wiberg, K.B., Walters, V.A., Wong, K.N. and Colson, S.D., J. Phys. Chem. 88, 6067 (1984).

B. Wilson Mode #'s for Benzene

C. Loss Peak Not Observed at This Frequency, Most Probably Hidden Under More Intense Loss Peak at 580 $cm^{-1}$.

References


1. a) Shanahan, K.L., and Muetterties, E.L., J. Phys. Chem. 88(10), 1996 (1984). b) Koel, B.E., Crowell, J.E., Mate, C.M., and Somorjai, G.A., J. Phys. Chem. 88 1988 (1984). These two publications have a complete reference list for benzene adsorbed on many different transition metals.

2. a) Demuth, J.E., Sanda, P.N., Warlaumont, J.M., Tsang, J.C., Christmann, K., "HREELS and SERS Studies of Pyridine and Benzene on Ag(111)", Vibrations at Surfaces, Ed. R. Caudana, J.-M. Giles, and A.A. Lucas, Plenum Press, N.Y. 391-410 (1982); b) Demuth, J.E., Christmann, K., and Sanda, P.N., Chem. Phys. Letts. 76(2), 201 (1980); c) DiNardo, J.N., Avouris, P., and Demuth, J.E., J. Chem. Phys. 81(4), 2169 (1984).

3. (a) Wexler, R.M., Tsai, M.-C., Friend, C.M., and Muetterties, E.L., J. Am. Chem. Soc. 104, 2034 (1982); b) Wexler, R.M., Ph.D. Thesis, University of California-Berkeley (1983).

4. Corrsin, L., Fax, B.J. and Lord, R.C., J. Chem. Phys. 21(7), 1170 (1953).

5. Wilmhurst, J.K. and Bernstein, H.J., Can. J. of Chem. 18, 1183 (1957).

6. Long, D.A. and Thomas, E.L., Trans. Faraday Soc. 59, 783 (1963).

7. DiLella. D.P. and Stidham, H.D., J. Raman Spec. 9(2), 90 (1980).

8. Wong, K.N. and Colson, S.D., J. Molec. Spec. 104, 129 (1984).

9. Gill, N.S., Nuttall, R.H., Scaife, D.E., and Sharp, D.W., J. Inorg. Nucl. Chem. 18, 79 (1961)

10. Durig, J., Mitchell, B.R., Sink, D.W., and Willis, J.N., Jr. Spectrochimica Acta. 23A, 1121 (1976).

11. a) Adams, D.M., Christopher, R.E., and Stevens, D.C., Inorg. Chem. 14, 1562 (1975); b) Schafer, L. and Southern, J.F., Spectrochimica Acta. 27A, 1083 (1971).

12. Howard, M.W., Dettle, S.F., Oxton, I.A., Powell, D.B., and Sheppard, N., J. Chem. Soc, Faraday Trans. 2, 77, 397 (1981).

13. Skinner, P., Howard, M.W., Oxton, I.A., Kettle, S.F., Powell, D.B., and Sheppard, N., J. Chem. Soc. Faraday Trans. 2, 77, 1203 (1981).

14. Shapley, J.R., George, G.M., Churchill, M.R., and Hollander, F.J., Inorg. Chem. 21, 3295 (1982).

15. Dubois, L., Ph.D. Thesis, University of California-Berkeley (1981).

16. a) Muetterties, E.L. and Tsai, M.-C., Bull. Soc. Chim. Belg. 89, 813 (1980); b) Tsai, M.C., Ph.D. Thesis, University of California-Berkeley (1982).

17. Wexler, R.M. and Muetterties, E.L., J. Phys. Chem. 84(18), 4037 (1984).

18. Bak, B., Hansen, L., Rastrup-Anderson, J., J. Chem. Phys. 22, 2013 (1985).

19. Yin, C.-C. and Demming, A.J., J.C.S. Dalton, 2091 (1975).

20. Johnson, B.F.G., Lewis, J., and Pippard, D.A., J.C.S., Dalton, 407 (1981).

21. Kettle, S.F.A. and Strangellin, P.L., Inorg. Chem. 18 2749 (1979).

22. Lehwald, S., Ibach, H., and Demuth, J.E., Surface Science 78 478 (1977).

23. Unpublished results this laboratory. The high resolution electron energy loss spectrum of toluene adsorbed on Pt(111) at room temperature is very similar to the room temperature spectrum of benzene on Pt(111). The methyl group in toluene does not seem to cause the molecule to distort from the benzene structure.

24. Davis, S.M., Gordon, B.E., Press, M., and Somorjai, G.A., J. Vac. Sci. and Technol. 19 231 (1981).

25. Johnson, A.L., Muetterties, E.L., Stohr, J., and Sette, F., J. Phys. Chem. 89(19), 4071 (1985).

26. Redhead, P.A., Vacuum 12 203 (1962).

FIGURE CAPTIONS

Fig. 1. The infrared spectrum of $HOs(CO)_{10}NC_5H_4$ and $Os(CO)_{11}NC_5H_5$ (and the perdeuterated compounds) in the region of 400-1600 $cm^{-1}$. (a) perhydro compounds, (b) perdeutero compounds.

Fig. 2. Electron energy loss spectrum of pyridine adsorbed on Pt(111) at room temperature and saturation coverage. (a) $NC_5H_5$, (b) $NC_5D_5$.

Fig. 3. The carbon-hydrogen and carbon-deuterium stretching frequency region for specifically labeled pyridines, $4d^1$ pyridine and $2,6d^2$ pyridine, with the normal and perdeuterated pyridine also shown for comparison.

Fig. 4. Thermal desorption spectrum for pyridine adsorbed on Pt(111) at room temperature (monitoring the parent ion AMU = 79) for molecular desorption. The heating rate for all thermal desorption experiments was 25-30 deg/sec.

Fig. 5. Electron energy loss spectrum of pyridine (and perdeuterated pyridine) adsorbed on Pt(111) at 120K and a coverage of one monolayer. (a) $NC_5H_5$, (b) $NC_5D_5$.

Fig. 6. Thermal desorption spectrum for reversible molecular desorption of pyridine adsorbed on Pt(111) at 120K as a function of coverage. Exposures noted are uncalibrated and in units of Langmuir's where 1 Langmuir = $1 \times 10^{-6}$ torr-sec.

Fig. 7. Thermal desorption spectrum (monitoring AMU=2) for hydrogen evolution. Three hydrogen peaks are observed with temperature maxima of 335K, 515K, and 620K.

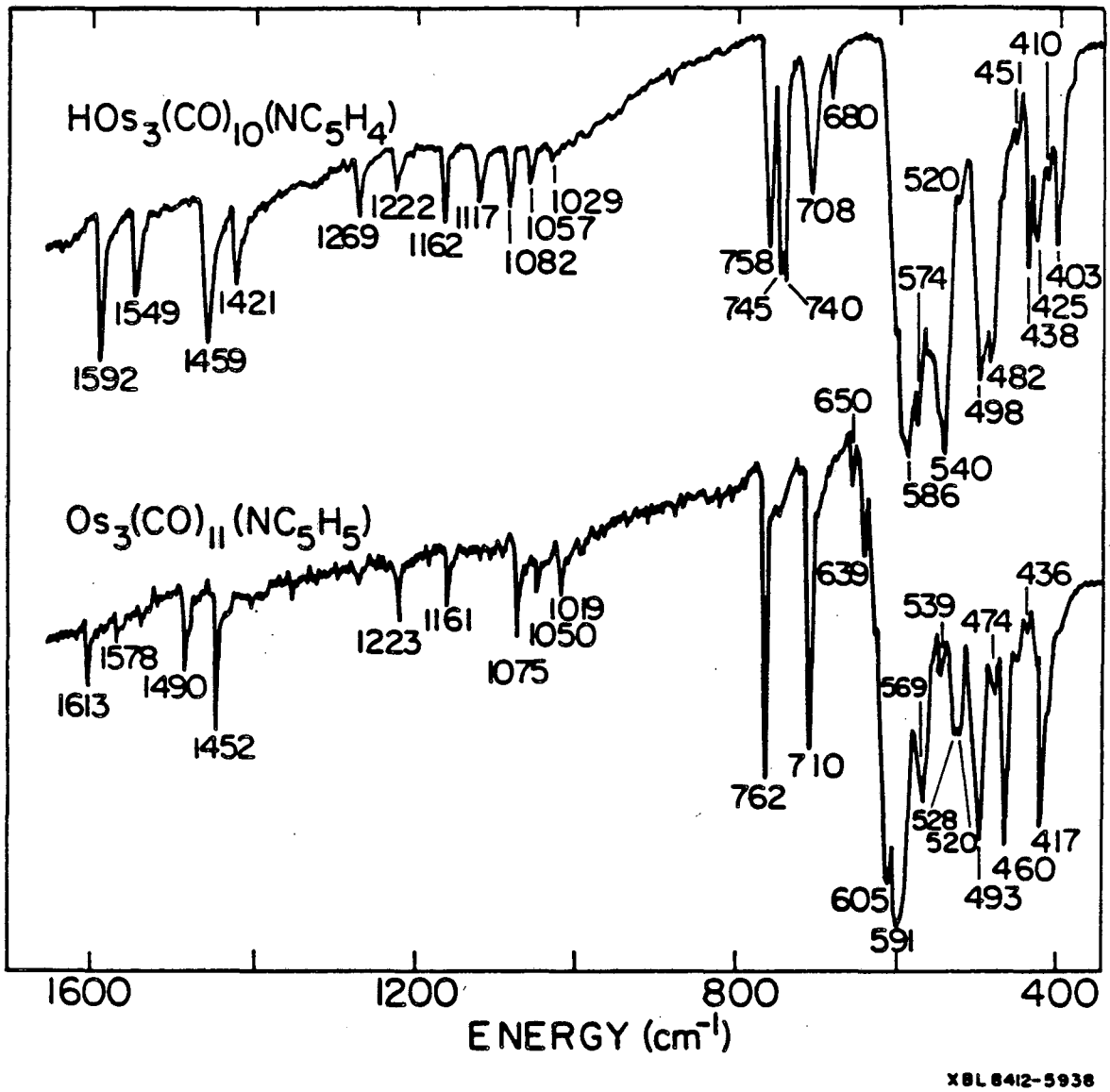
HOs3(CO)10(NC5H4)
1592
1549
1459
1421
1269
1222
1162
1117
1082
1057
1029
758
745
740
708
680
574
540
586
520
498
482
451
438
425
410
403
Os3(CO)11(NC5H5)
1613
1578
1490
1452
1223
1161
1075
1050
1019
762
710
650
639
605
591
569
539
528
520
493
474
460
436
417
1600
1200
800
400
ENERGY (cm-1)
XBL 8412-5938

Fig. 1a

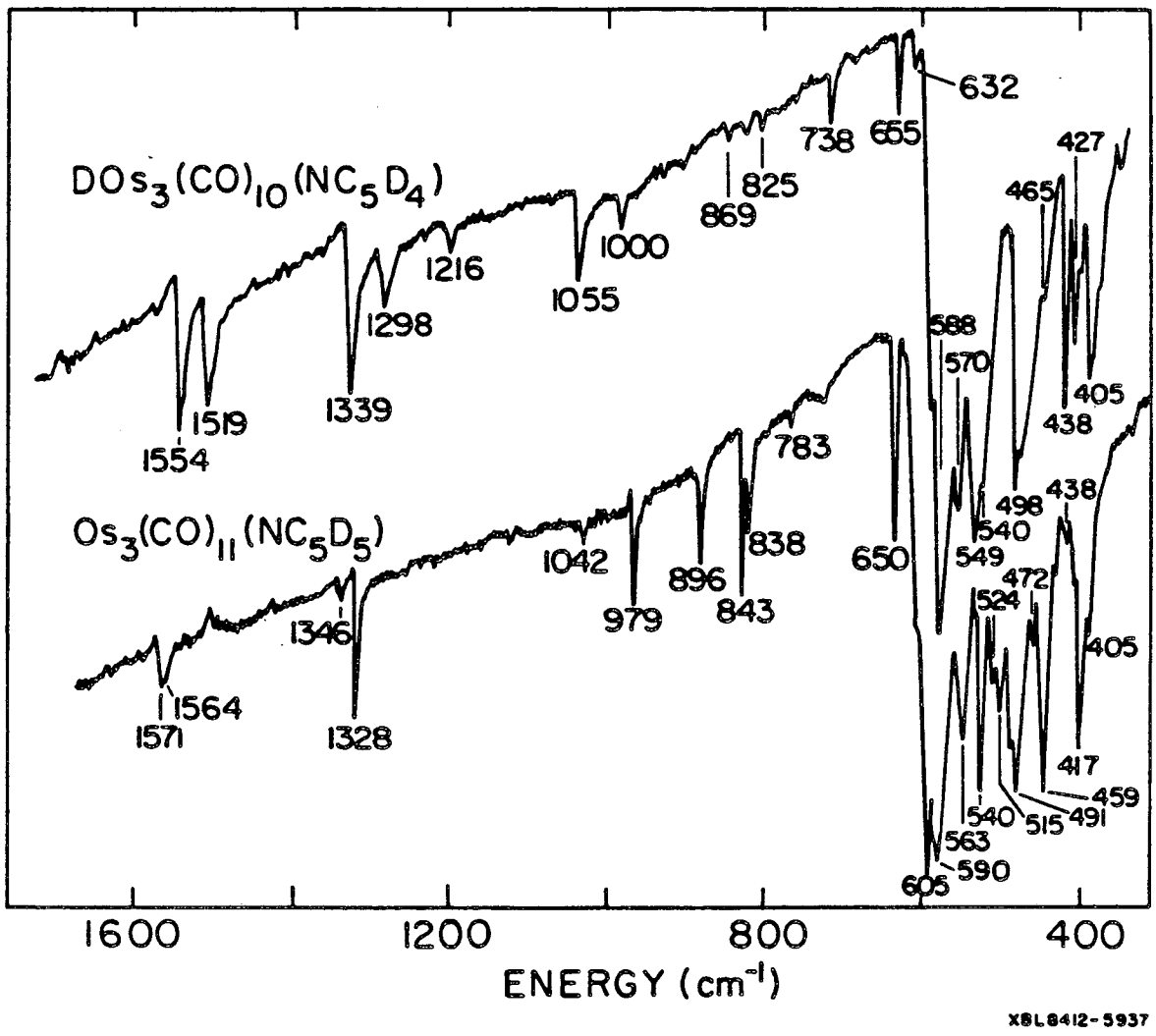
DOs3(CO)10(NC5D4)
1554
1519
1339
1298
1216
1055
1000
869
825
738
665
632
427
465
405
438
588
570
Os3(CO)11(NC5D5)
1571
1564
1346
1328
1042
979
896
843
838
783
650
498
540
549
472
524
438
405
417
459
491
515
540
563
590
605
1600
1200
800
400
ENERGY (cm-1)
XBL8412-5937

Fig. 1b

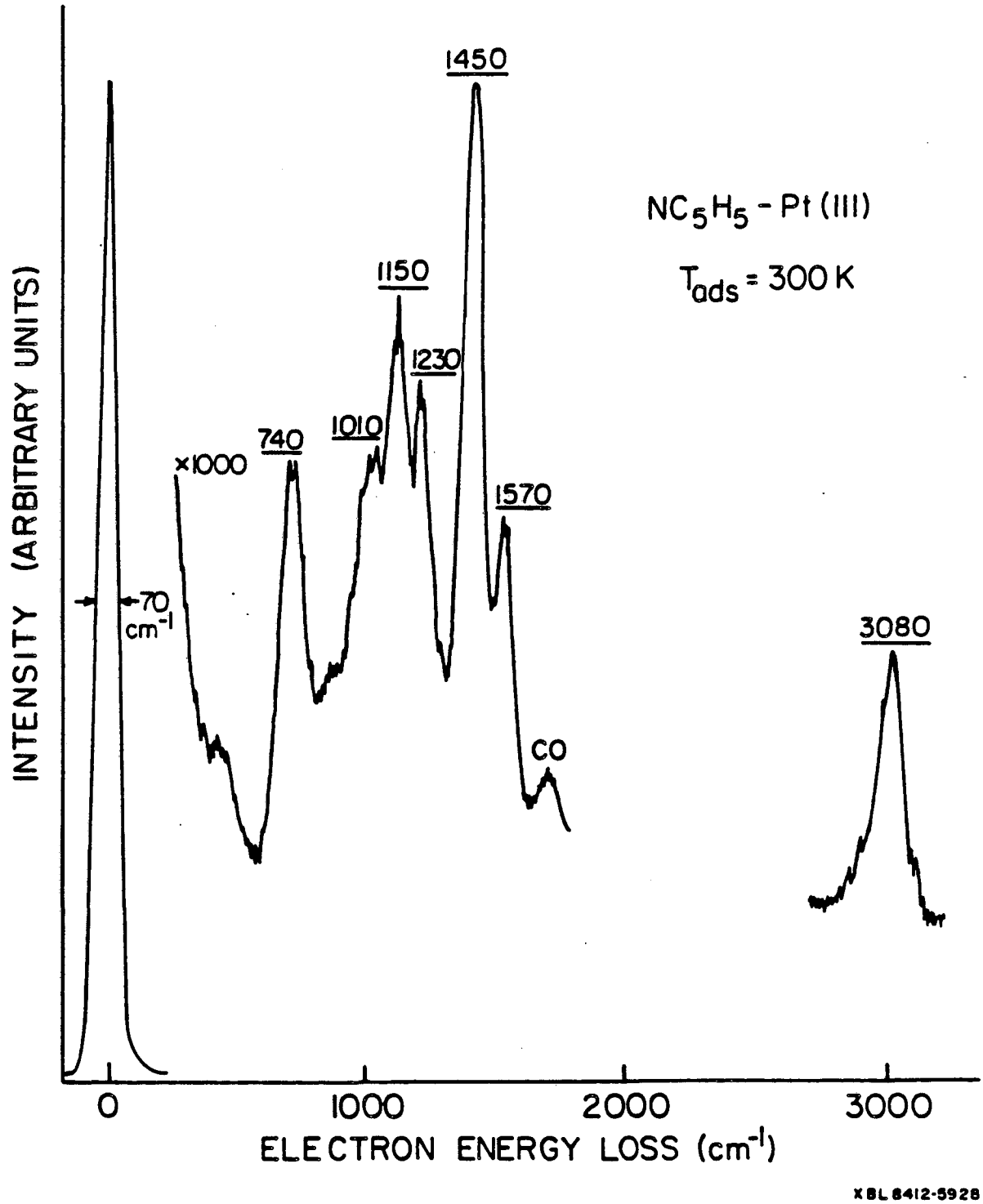
1450
1150
1230
1010
740
×1000
1570
3080
CO
70 cm⁻¹
NC5H5 - Pt (111)
Tads = 300 K
INTENSITY (ARBITRARY UNITS)
0
1000
2000
3000
ELECTRON ENERGY LOSS (cm⁻¹)
XBL 8412-5928

Fig. 2a

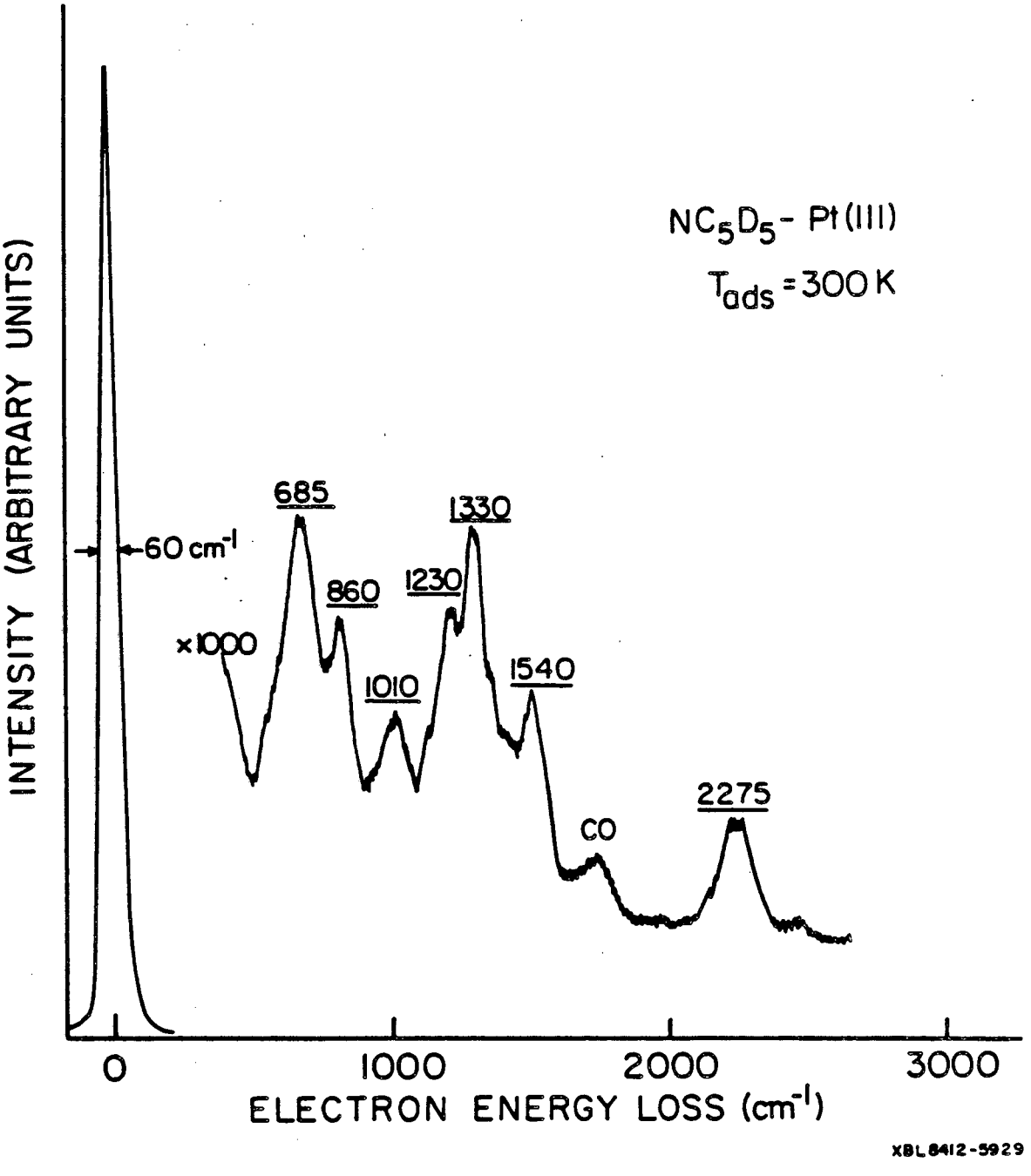
NC5D5 - Pt(111)
Tads = 300 K
INTENSITY (ARBITRARY UNITS)
60 cm-1
685
860
1010
1230
1330
1540
CO
2275
x1000
0
1000
2000
3000
ELECTRON ENERGY LOSS (cm-1)
XBL8412-5929

Fig. 2b

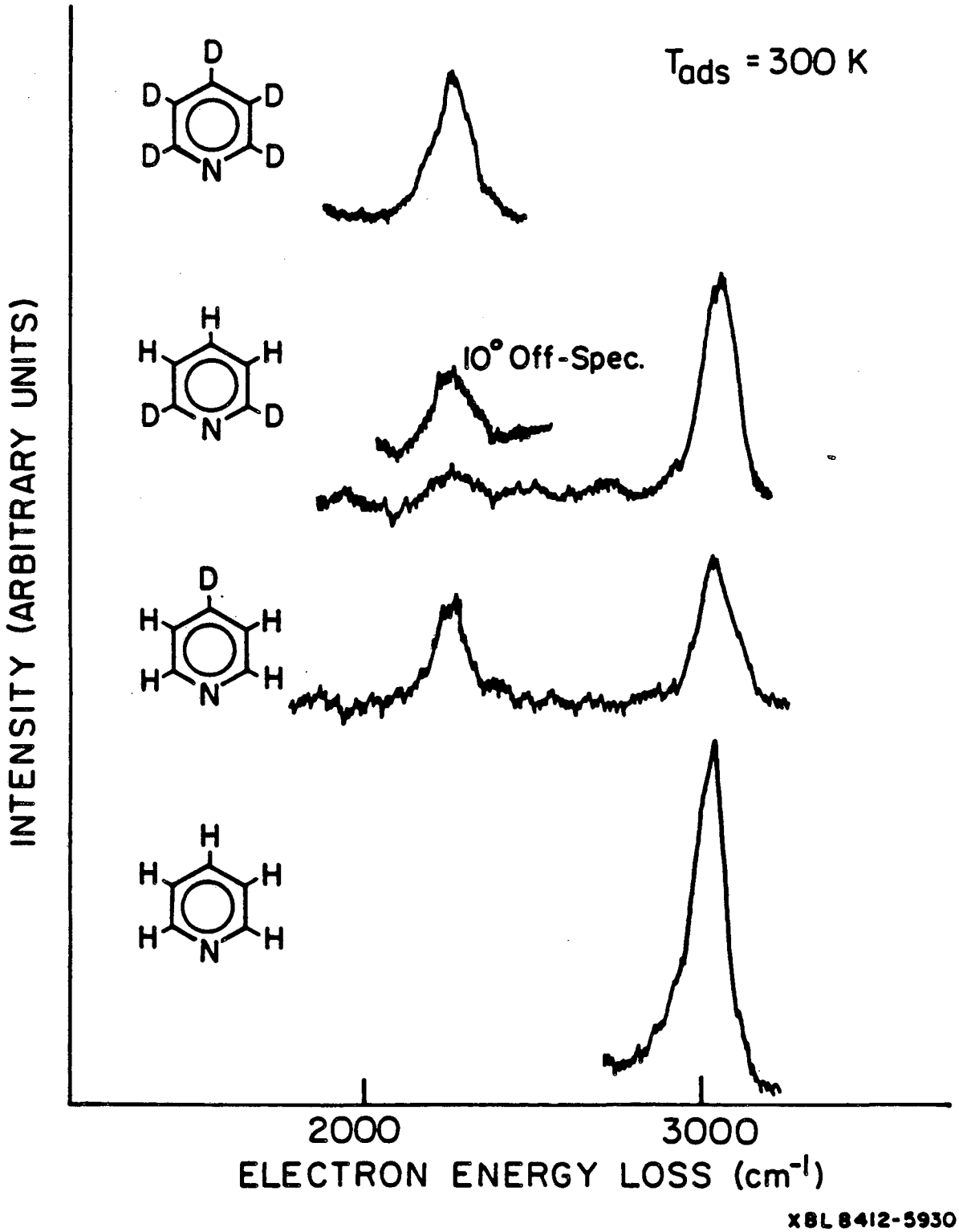
$T_{ads}$ = 300 K
10° Off-Spec.
INTENSITY (ARBITRARY UNITS)
2000
3000
ELECTRON ENERGY LOSS ($cm^{-1}$)
XBL 8412-5930

Fig. 3

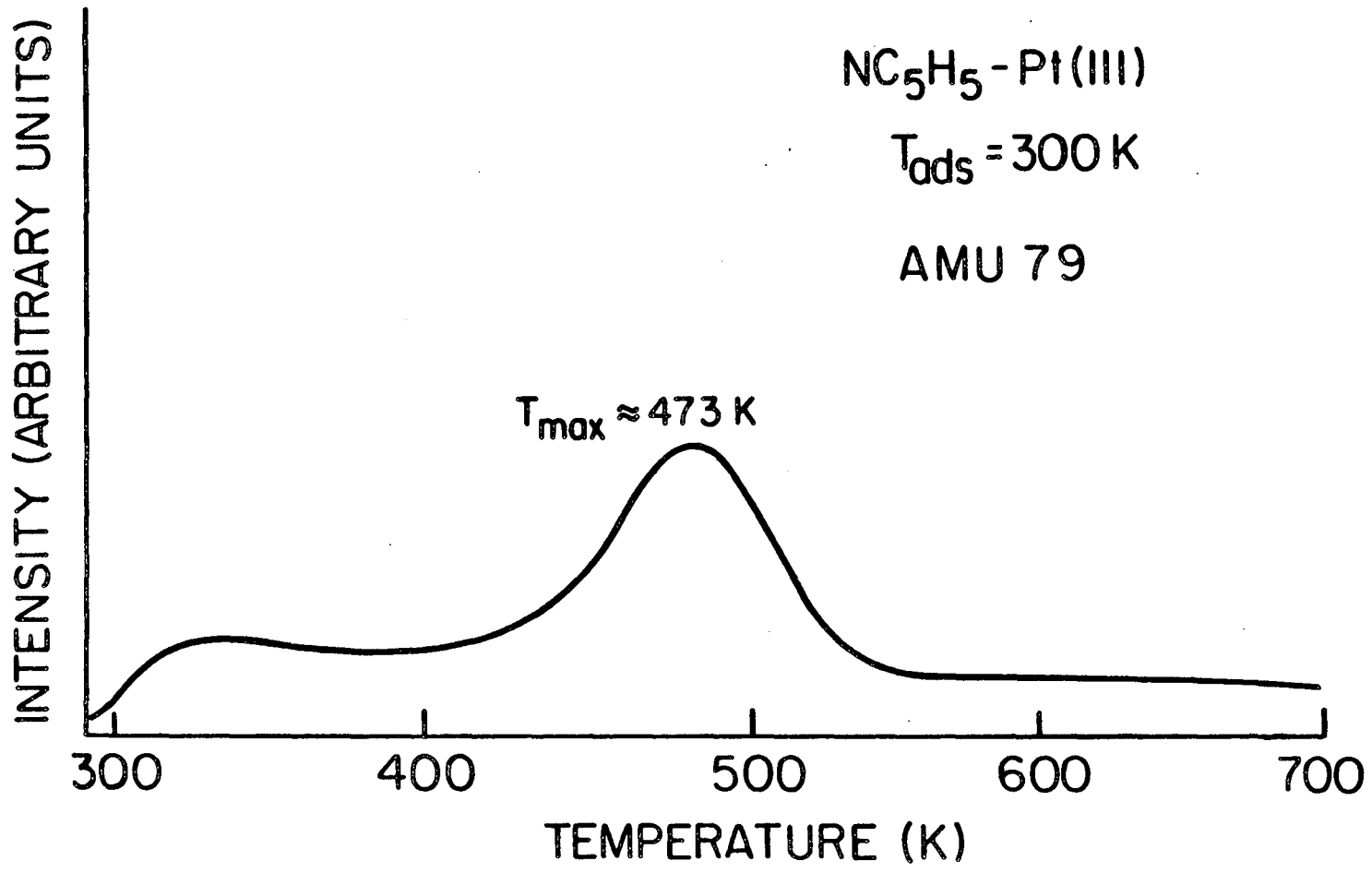
INTENSITY (ARBITRARY UNITS)
$NC_5H_5$ - Pt(111)
$T_{ads}$ = 300 K
AMU 79
$T_{max} \approx 473$ K
300
400
500
600
700
TEMPERATURE (K)
XBL 8412-5931

Fig. 4

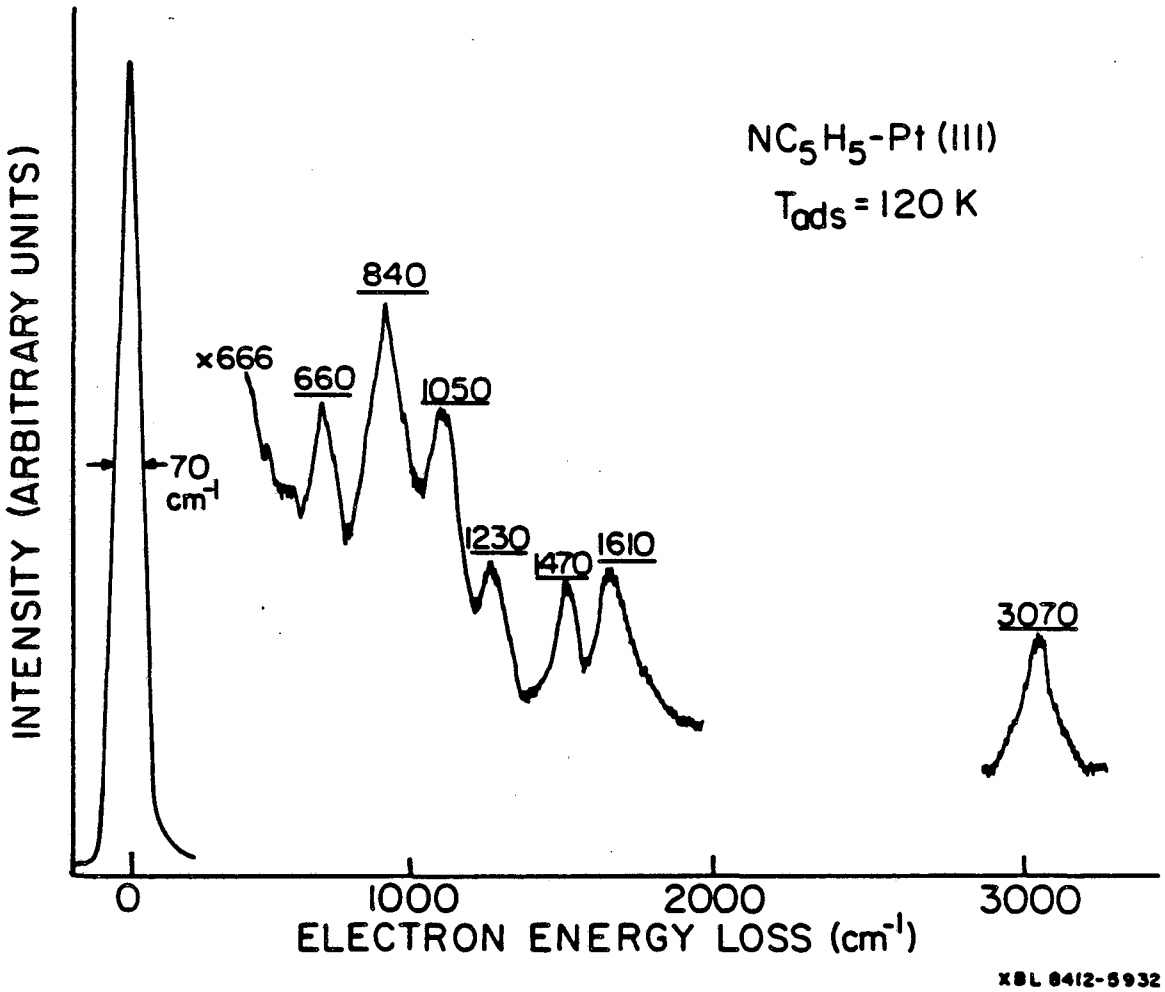
NC5H5-Pt (111)
Tads = 120 K
INTENSITY (ARBITRARY UNITS)
x666
840
660
1050
1230
1470
1610
3070
70 cm-1
0
1000
2000
3000
ELECTRON ENERGY LOSS (cm-1)
XBL 8412-5932

Fig. 5a

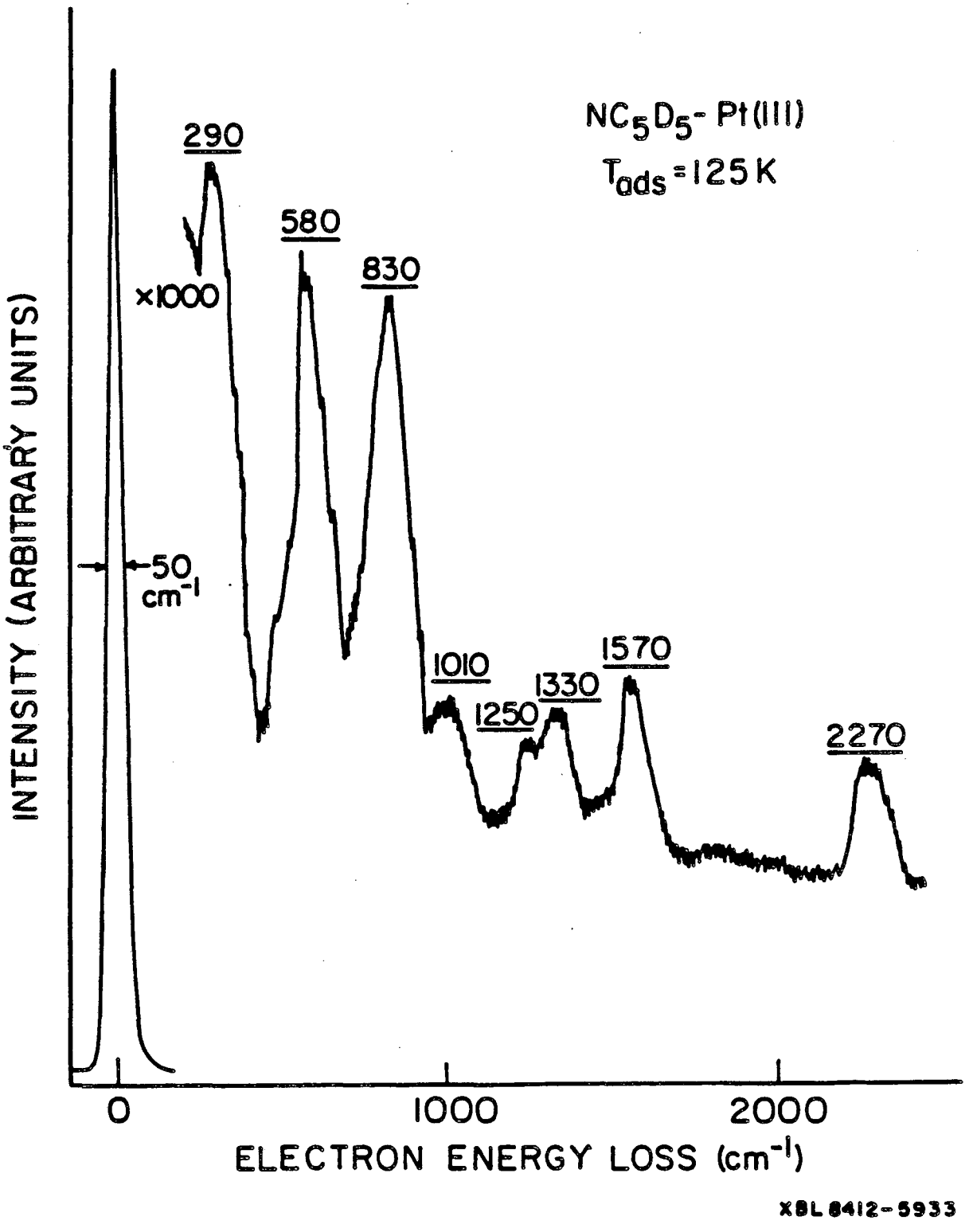
NC5D5- Pt(111)
Tads = 125 K
290
580
830
×1000
1010
1250
1330
1570
2270
50 cm-1
INTENSITY (ARBITRARY UNITS)
0
1000
2000
ELECTRON ENERGY LOSS (cm-1)
XBL 8412-5933

Fig. 5b

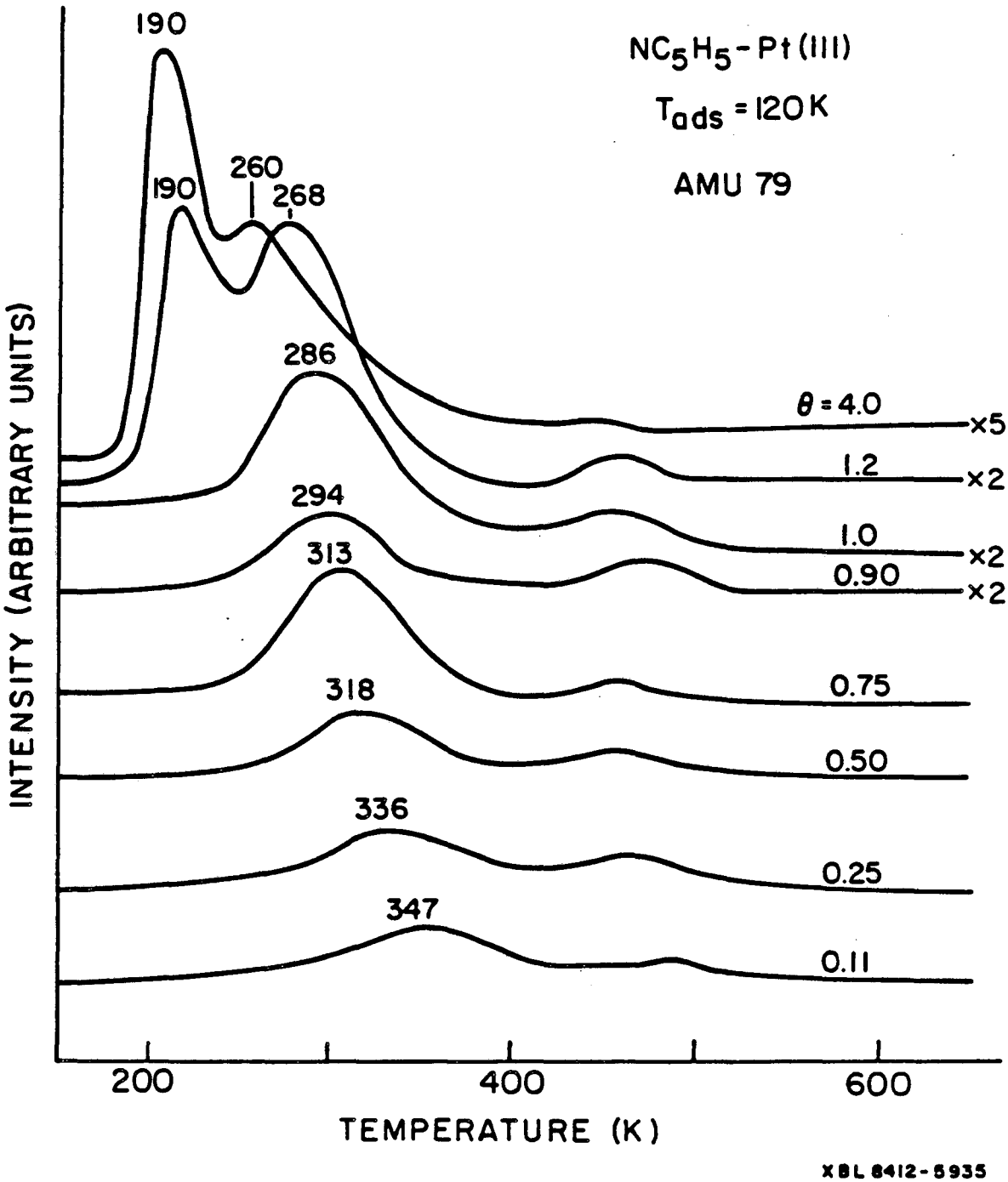
190
190
260
268
286
294
313
318
336
347
NC5H5 - Pt (111)
Tads = 120K
AMU 79
θ = 4.0
×5
1.2
×2
1.0
×2
0.90
×2
0.75
0.50
0.25
0.11
INTENSITY (ARBITRARY UNITS)
200
400
600
TEMPERATURE (K)
XBL 8412-5935

Fig. 6

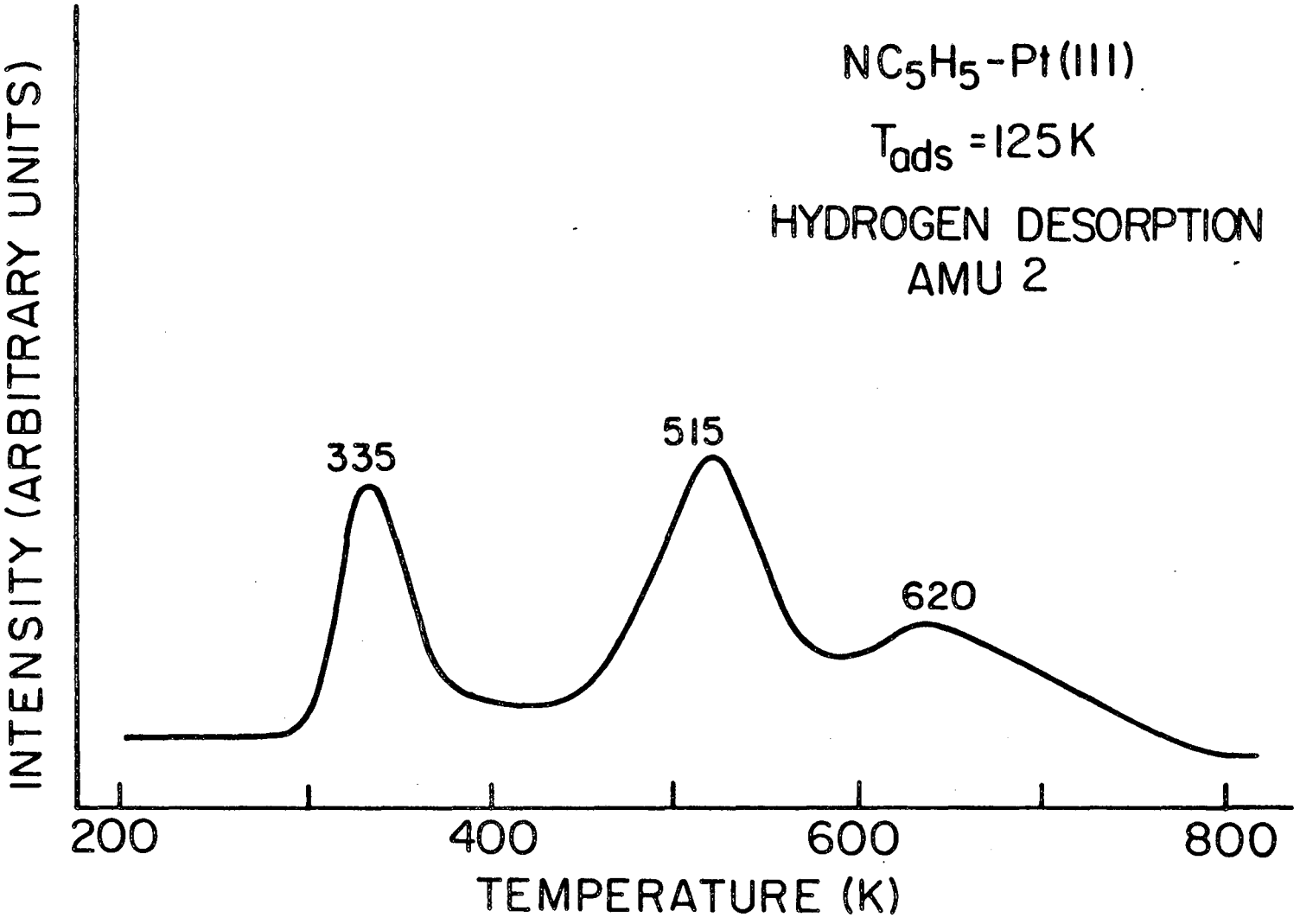


XBL 8412-5936

Fig. 7

*LAWRENCE BERKELEY LABORATORY*
*TECHNICAL INFORMATION DEPARTMENT*
*UNIVERSITY OF CALIFORNIA*
*BERKELEY, CALIFORNIA 94720*